SEOFP-NET: Compression and Acceleration of Deep Neural Networks for Speech Enhancement Using Sign-Exponent-Only Floating-Points

Yu-Chen Lin, Cheng Yu, Yi-Te Hsu, Szu-Wei Fu, Yu Tsao, *Senior Member, IEEE*, and Tei-Wei Kuo, *Fellow, IEEE*

***Abstract*—Numerous compression and acceleration strategies have achieved outstanding results on classification tasks in various fields. Nevertheless, the same strategies may yield unsatisfactory performance on regression tasks because the nature between regression and classification tasks differs. In this paper, a novel sign-exponent-only floating-point network (SEOFP-NET) technique is proposed to compress the model size and accelerate the inference time for speech enhancement, a regression task of speech signal processing. The proposed method compressed the sizes of deep neural network (DNN)-based speech enhancement models by quantizing the fraction bits of single-precision floating-point parameters during training. Before inference implementation, all parameters in the trained SEOFP-NET model are adjusted to accelerate the inference time by replacing the floating-point multiplier with an integer-adder. The experimental results indicate that the size of SEOFP-NET models can be significantly compressed by up to 81.249% without noticeably downgrading their speech enhancement performance, and the inference time can be accelerated to 1.212x compared with the baseline models. The results also verify that SEOFP-NET can cooperate with other efficiency strategies to achieve a synergy effect for model compression. In addition, results of a just noticeable difference experiment show that the listeners cannot facilely differentiate between the enhanced speech signals processed by the baseline model and SEOFP-NET. To the best of our knowledge, this study is one of the first works that aims to compress the model size and reduce the inference time of speech enhancement while maintaining satisfactory performance. The promising results confirm the potential applicability of SEOFP-NET to lightweight embedded devices.**

***Index Terms*—Speech enhancement, speech dereverberation, deep neural network model compression, inference acceleration, floating-point integer arithmetic circuit.**

Manuscript received May 7, 2021; revised September 3, 2021 and October 22, 2021; accepted November 23, 2021. Date of publication December 13, 2021; date of current version March 9, 2022. This work was supported by Academia Sinica Career Development Award AS-CDA-106-M04. The Associate Editor coordinating the review of this manuscript and approving it for publication was Prof. Tom Bäckström. *(Corresponding author: Yu Tsao.)*

Yu-Chen Lin, Cheng Yu, Szu-Wei Fu, and Yu Tsao are with the Research Center for Information Technology Innovation, Academia Sinica, Taipei 11529, Taiwan (e-mail: f04922077@csie.ntu.edu.tw; chengyu_citi@citi.sinica.edu.tw; d04922007@ntu.edu.tw; yu.tsao@citi.sinica.edu.tw).

Yi-Te Hsu is with the Department of Computer Science, Johns Hopkins University, Baltimore, MD 21287 USA (e-mail: b01901112@ntu.edu.tw).

Tei-Wei Kuo is with the Department of Computer Science and Information Engineering, National Taiwan University, Taipei 10617, Taiwan, and also with the College of Engineering, City University of Hong Kong, Kowloon Tong, Hong Kong (e-mail: ktw@csie.ntu.edu.tw).

Digital Object Identifier 10.1109/TASLP.2021.3133209

I. Introduction

In RECENT years, many applications in different fields have widely used deep neural network (DNN)-based approaches. These networks can perform well because their deep structures enable DNN-based algorithms to efficiently derive characteristic features while executing various classification and regression tasks. Many studies have verified that DNN-based algorithms outperform traditional techniques in different computer vision and speech signal processing domains, such as image detection [1], [2], object detection [3]–[5], speech recognition [6]–[12], speaker recognition [13]–[15], and speech enhancement [16]–[27]. However, owing to their deep structures, most DNN-based algorithms require large memory spaces and incur high computing costs. As a result, many hardware companies have developed high-level computing units, such as graphics processing units [28]–[30], to satisfy the requirements of memory and computation. In addition to personal computers and mainframes, researchers have aimed to employ DNN-based algorithms to applications in embedded devices used around people. In this Internet-of-Things era, the number of small embedded devices has exponentially increased. Such devices cannot be equipped with large storage and high-level computing units. That is, the applications in embedded devices can only use DNN-based algorithms by accessing DNN models on remote servers through network connections. However, the latency or disconnection of wireless communication influences the requirements of real-time predictions. Accordingly, researchers have attempted to locally install DNN-based algorithms in embedded devices.

To implement DNN-based algorithms in embedded devices, the algorithms must be compressed, and computational costs must be reduced. To resolve this problem, many researchers have successfully developed various compression methods [31]–[36]. The BinaryConnect algorithm [31], which uses 1-bit wide weights in the DNN model, yields satisfactory performance in image classification tasks on various image datasets (e.g., MNIST [37], CIFAR-10 [38], and SVHN [39]). Gong *et al.* [32] compressed deep convolutional neural networks (CNNs) using vector quantization. The primeval weights in the models are replaced by the centroid values through the proposed clustering method. This method only results in a 1% loss of classification accuracy for state-of-the-art CNNs. The incremental network quantization (INQ) [33] converts pre-trained full-precision CNN models into a low-precision version. The weights in the CNN models are all constrained to be either powers of two or zero. Several experiments on image classification tasks over different

well-known CNN architectures (e.g., AlexNet [40], VGGNet [1], and GoogleNet [41]) have been conducted. The experimental results show that the proposed INQ method achieves slightly better performances in the top-1 and top-5 errors using 5-bit quantization. Most of these compression methodologies have been clearly observed as implementable in classification-based DNN models, such as image recognition [32]–[34] and speech recognition [42]–[47], which classify the input data into a set of output categories. In contrast, for regression tasks, the output has continuous values. In brief, the output form of regression tasks considerably differs from that of classification tasks. Among the existing techniques, Ko *et al.* [47] proposed a precision scaling method for neural networks to achieve efficient audio processing. They conducted several experiments on both speech recognition (classification task) and speech enhancement (regression task). The experimental results showed that the proposed technique exhibited unsatisfactory performance on speech enhancement but acceptable performance on speech recognition. Sun *et al.* [48] developed an optimization method for DNN-based speech enhancement models by utilizing a weight-sharing technique for model compression. Their experimental results showed that although the size of the DNN model was compressed, the speech enhancement performance was clearly degraded. Hence, even though the foregoing techniques can efficiently reduce the DNN model size, they also degrade the model performance on speech signal processing regression tasks, such as speech enhancement. That is, regression tasks compared with classification tasks are more sensitive to value changes in the parameters of DNN-based models.

In the present work, a novel sign-exponent-only floating-point network (SEOFP-NET) is proposed. It is a neural network whose parameters are represented by a sign-exponent-only floating-point for model compression and inference acceleration of speech enhancement tasks. Hence, it is an extremely useful application for speech signal processing. The proposed SEOFP-NET compresses DNN-based speech enhancement models by quantizing the fraction bits of the original single-precision floating-point representation. After training, all parameters in the trained SEOFP-NET model are slightly adjusted to accelerate the inference time by replacing the floating-point multiplier logic circuit with an integer-adder logic circuit. For generalization, several experiments were conducted on two important regression tasks in speech enhancement (i.e., speech denoising and speech dereverberation) with two different model architectures (bidirectional long short-term memory (BLSTM) [49], [50] and a fully convolutional network (FCN) [51])) under two common corpora (TIMIT [52] and TMHINT [53]). To evaluate the enhancement performance, standardized objective evaluation metrics, including the perceptual evaluation of speech quality (PESQ) [54] and short-time objective intelligibility measure (STOI) [55], were employed. The experimental results illustrate that the size of the SEOFP-NET model can be substantially compressed by up to 81.249% without considerably downgrading the enhancement performance. Moreover, the inference time can be accelerated to 1.212$\times$ compared with that of baseline models. The result also verifies that our SEOFP quantization can cooperate with other efficiency strategies to achieve a synergy effect. In addition, for the user study experiment, the just noticeable difference (JND) [56]–[58] was employed to analyze the effect of speech enhancement on listening. The experimental results indicate that the listeners cannot effortlessly differentiate between the speech signals enhanced by the baseline model and SEOFP-NETs. To the best knowledge of the authors, this study is one of the first works that considerably compresses the size of DNN-based algorithms and reduces the inference time of speech enhancement tasks simultaneously while maintaining satisfactory enhancement performance. These promising results suggest that the application of DNN-based speech enhancement algorithms to various lightweight embedded devices using the proposed SEOFP-NET technique is advantageous.

The remainder of this paper is organized as follows. In Section II, the background knowledge on speech enhancement and floating-point-based parameters of DNN-based algorithms is first presented; the research motivation is explained thereafter. Section III elaborates on the size compression of DNN-based models and the acceleration of the inference time of trained models using the proposed SEOFP-NET methodology. Section IV describes the conduct of experiments in the study with various datasets and different speech enhancement tasks to illustrate the generalization of the proposed SEOFP-NET algorithm. The disentanglement measurements with various metrics and the relevance of the SEOFP-NET algorithm to speech enhancement are also presented in this section. Finally, Section V concludes the paper and discusses future work.

II. Background and Motivation

In Sections II-A and II-B, two important speech enhancement tasks in regression of speech signal processing, i.e., speech denoising and dereverberation, are introduced, respectively. In Section II-C, the background knowledge on the single-precision floating-point representation, which is commonly used in DNN-based models, is discussed. Next, in Section II-D, the electronic circuits of multiplication operation are introduced based on the aforementioned representation. Finally, in Section II-E, a preliminary experiment is presented, and the motivation of this work is explained.

A. Speech Denoising

The purpose of speech denoising is to generate improved speech and remove noise from an original speech composed of clean speech and environmental noise. Traditionally, speech denoising is carried out on the time-frequency magnitude spectrograms of speech signals [49], [50], [59]–[64]. This implies that the raw noisy speech waveform is converted to the magnitude spectrogram of noisy speech before denoising is implemented. After denoising, the processed magnitude spectrogram is converted back to waveform. Most spectrogram mapping-based algorithms facilely use the phase of the noisy speech to rebuild the waveform of the denoised speech. Recently, a number of researchers have proposed the use of waveform mapping-based techniques [65]–[72] to denoise speech in the waveform domain without waveform-spectrogram conversion. In this study, the proposed SEOFP-NET is applied to both spectrogram and waveform mapping-based speech denoising algorithms to illustrate its generalizability.

In recent years, DNN models have been widely used in speech denoising tasks. Generally, a DNN-based speech denoising model comprises two phases: offline training and online inference. In the offline training phase, numerous noisy speech signals consisting of various clean speech signals and types of noise exist in the training corpus. These noisy speech signals in the training corpus are alternately supplied to the DNN-based speech denoising model, which then generates enhanced speech

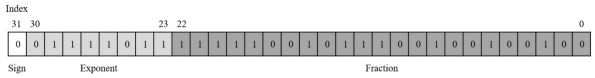

Fig. 1. An example of the IEEE-754 single-precision floating-point representation. The binary format are divided into three parts: $sign$, $exponent$, and $fraction$. The decimal value of this binary example is 0.123400 corrected to six decimal places.

based on the original noisy speech. To determine the difference between the two utterances, various criteria, such as the mean square error (MSE) [49], [59]–[61], L1 norm [67], and STOI [66], are selected as measurement standards. After measurements, all parameters in the DNN-based model are updated according to the evaluated difference. By contrast, in the online inference phase, noisy speech containing mismatching clean utterances and noise is supplied to the trained denoising model. Ultimately, the denoising system generates an enhanced speech based derived from noisy speech. Although the two phases are similar among different DNN-based denoising systems, various models, such as deep denoising autoencoders (DDAEs) [59], [62], CNNs [61], [64], FCNs [65]–[68], and BLSTMs [49], [50], may be applied. In this work, to illustrate the generalization of the proposed technique, the SEOFP-NET is primarily applied to two model architectures, BLSTM and FCN.

B. Speech Dereverberation

Speech reverberation is defined as the combination of speech signal and its multiple reflections from objects or surfaces within a given space. Speech reverberation has been confirmed to cause severely degraded speech quality and intelligibility defects. Hence, reverberation can considerably affect certain speech-related applications, such as automatic speech recognition [9]–[12],[6], [8] and speaker identification [13]–[15]. Reverberation also considerably affects all listeners, normal and impaired. For decades, researchers have proposed numerous approaches to address the reverberant issue. Conventional dereverberation techniques include the minimum mean square error [73], beamforming [74], and matched filtering [75].

With the rapid developments in the deep learning methods over the past decade, the application of non-linear approaches for dereverberation tasks has been proposed. DNNs or deep fully connected networks with direct mapping methods have been proposed to improve speech-related system performance through the learning capabilities of deep structured networks. Some researchers have proposed to using DNNs [76], [77] to recover anechoic speech signals from their reverberated counterpart.

C. Single-Precision Floating-Point Representation in DNN Models

The DNN models for either speech denoising or dereverberation contain a considerable number of parameters. Most of these systems use the IEEE-754 single-precision floating point [78] to represent the parameters; Fig. 1 shows the binary representation of this floating point. The binary format has three parts: $sign$, $exponent$, and $fraction$ (also known as significand or mantissa). The sign part has only one bit, i.e., $bit[31]$, which is regarded as the most important bit in the entire 32-bit binary representation; it indicates the sign of the floating-point value

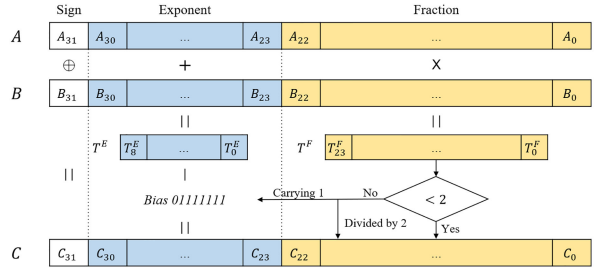

Fig. 2. Multiplication of two floating-point values A and B. The sign bit C_{31} is the result of XOR operation of A_{31} and B_{31}. The exponent bits C_{30-23} are the addition result of A_{30-23} and B_{32-23} with consideration of carrying condition from fraction part. The fraction bits C_{22-0} are the multiplication result of unsigned A_{22-0} and B_{22-0}.

(0 for positive and 1 for negative). The exponent part has eight bits, i.e., $bit[30-23]$, denoting an unsigned integer, which is the number of times the power of two is raised. The fraction part has 23 bits, i.e., $bit[22-0]$, representing a real number. Similar to scientific notation, the decimal value of a single-precision floating point is indirectly calculated using Equation 1.

$$(value)_{10} = (-1)^{sign} \times (fraction)_{10} \times 2^{(exponent)_{10}-bias}. \tag{1}$$

Owing to the unsigned integer feature, a $bias$ is necessary for shifting the value range of the exponent. In the single-precision floating-point format, the $bias$ for an 8-bit unsigned exponent is 127 (2^7-1), shifting the value range of the exponent from [0, 255] to [−127, 128]. In addition, the decimal value of the fraction part can be calculated using the following equation.

$$(fraction)_{10} = 1 + \sum_{i=0}^{22} bit[i] \times 2^{i-23} \tag{2}$$

For instance, consider the binary representation in Fig. 1 in which the $sign$ is 0, the 8-bit $exponent$ is 01111011, and the 23-bit $fraction$ is 11111001011100100100100. It can be calculated using the following equation.

$$value = (-1)^0 * (1.9744\ldots) * 2^{123-127} \approx 0.123400 \tag{3}$$

The equation yields the decimal value 0.123400, which is correct to six decimal places.[1]

D. Arithmetic Electronic Circuits

Fig. 2 illustrates a single-precision floating-point multiplier circuit that operates the multiplication of two single-precision floating-point values: $A \times B = C$. For the sign part, two operands, $A[31]$ and $B[31]$, execute an exclusive OR operation to obtain the output sign, $C[31]$, of the result value, C. For the exponent part, two unsigned integers, $A[30-23]$ and $B[30-23]$, first execute an addition operation to obtain a temporary 9-bit output value, $T^E[8-0]$ The main reason for the 9-bit width is to cope with $overflow$. The value range of the addition of two 8-bit unsigned operands whose value range is [0, 255] becomes [0, 510]; consequently, the temporary value, $T^E[8-0]$ requires at least 9 bits to receive the output. The $bias$ of the single-precision floating-point mentioned in Section II-C, i.e., 127, is

[1]For understanding the conversion from binary to decimal value in detail, please consult https://www.exploringbinary.com/floating-point-converter.

TABLE I
A PRELIMINARY EXPERIMENT ON DNN-BASED SPEECH DENOISING UNDER THREE KINDS OF BIT-WIDTH IN THE FRACTION OF THE MODEL PARAMETERS. THE MASK BIT-LENGTH REPRESENTS THE NUMBER OF BITS THAT ARE MASKED BY 0 S IN THE END OF THE FRACTION

Mask Bit-length	Binary	Decimal	PESQ
0	0011...1100100100100	0.123400002718...	2.1435
6	0011...1100100**000000**	0.123399734497...	2.1352
12	0011...1**000000000000**	0.123382568359...	2.1413

then subtracted from the temporary output value, $T^E[8-0]$. Considering $32.0 \times 8.0 = 256.0$ as example, the exponent of 256.0 is 10000111 which is calculated by the following:

$$10000111 = 10000100 + 10000010 - 01111111 \quad (4)$$

where 10000100, 10000010 and 01111111 are the binary exponents, 32.0 and 8.0, and the single-precision floating-point $bias$, respectively. For the fraction part, two 23-bit values, $A[22-0]$ and $B[22-0]$, first execute a multiplication operation to obtain a temporary 24-bit output value, $T^F[23-0]$. Similar to the exponent part, the reason for the 24-bit width is to cope with $overflow$. According to Equation 2, the original value range of the fraction part is [1, 2); however, after multiplication, the value range becomes [1, 4). As a result, the temporary value, $T^F[23-0]$, requires 24 bits to receive the output. An if-else decision process determines whether or not $T^F[23-0]$ is less than 2. If it is not less than 2, then $T^F[23-0]$ is divided by 2. The quotient is then carried to the result exponent, $C[30-23]$, and the remainder is considered as the result of the 23-bit fraction, $C[22-0]$.

E. Preliminary Experiment and Motivation

Among the three parts of the single-precision floating-point format, the sign and exponent segments are clearly designed for the value range of the floating-point, and the fraction segment is designed for the value precision. In the past, precision has been a critical problem for many applications. Most bits in the single-precision floating-point representation are used for the fraction part (i.e., 23 bits in a 32-bit binary value). Recently, the single-precision floating-point format has been used in emerging DNN-based algorithms, as mentioned in Section II-C. However, the necessity of this format to DNN-based speech enhancement algorithms has to be ascertained. Accordingly, a preliminary experiment is conducted on a BLSTM-based denoising system; the experimental results are summarized in Table I. All parameters of the BLSTM model are directly masked by several 0 s at the end. Two bit lengths for the mask are used: 6 and 12. The row of the 0-bit mask represents the original denoising model with unmasked parameters. Based on the results in the table, the downgrade of the PESQ metric scores compared with those of the original model was not distinctly observed. In addition, these scores increased from a 6-bit mask to a 12-bit mask. These results motivated the authors to quantize the fraction part of all single-precision floating-point parameters of DNN-based speech enhancement systems.

Moreover, for executing arithmetic operations, the electronic circuits can be classified into two types: integer and floating point. In other words, many circuits, such as adders, subtractors, multipliers, and dividers are designed for integer arithmetic, whereas some circuits are designed for floating-point arithmetic. According to Section II-D and Fig. 2, the floating-point multiplier is composed of several sub-circuits of integer arithmetic. However, many other floating-point circuits also have the same feature, indicating that the circuits for integers are more efficient than the circuits for the floating-point in executing arithmetic operations. In addition, among the arithmetic circuits for integers, complicated circuits are designed based on simple yet efficient circuits. Consider the multiplier and divider as examples. The integer multiplication is completed by several additions, whereas the integer division is completed by several subtractions. This feature motivated the authors to use simpler and more efficient arithmetic circuits (e.g., integer adder or subtractor) to execute complicated arithmetic operations (e.g., floating-point multiplication or division) for the online inference phase of DNN-based speech enhancement systems. Using this method, the inference time of DNN models can be accelerated while performing speech enhancement.

However, several design challenges are raised by this scheme. First, the quantized limitation of the fraction part of the single-precision floating-point format has to be determined, allowing the quantized DNN models to achieve enhancement performance similar to that of the original single-precision model. Next, before replacing the complicated and inefficient arithmetic circuits with simpler and more efficient alternatives, the three parts of the floating-point parameter have to be adjusted for the arithmetic results to be the same as those of the original arithmetic operations.

III. SEOFP-NET

This section presents the proposed SEOFP-NET technique for DNN-based speech enhancement algorithms. Section III-A introduces the overall training procedure and model architecture of SEOFP-NET. Section III-B elaborates on the philosophies and algorithm of fraction quantization; it also presents the quantized limitation of the fraction part of the single-precision floating-point format to avoid the severe degradation of speech denoising or dereverberation performance. Section III-C expounds on the adjustment of the single-precision floating-point parameters of the models to replace the complicated and inefficient floating-point multiplier with a simpler and more efficient integer adder. Finally, the quantization of the exponent part after training to further compress the model size is discussed in Section III-D.

A. System Overview of SEOFP-NET Quantization

To quantize the fraction part of single-precision floating-point parameters, several bits at the end of the fraction part may be instinctively masked. Similar to the method employed in the preliminary experiment (Table I, Section II-E), this may be performed after training a DNN-based speech enhancement model, such as the post-training quantization in Tensorflow Lite [79]. However, casually modifying the parameters of a well-trained DNN model will affect either the accuracy of a classification task or the performance of a regression task. The main reason is that this parameter modification does not take the performance change into consideration. In other words, this intuitive quantization method may considerably degrade the speech enhancement performance. quantize model parameters while minimizing the influence of task performance, quantization should be implemented during training. Accordingly, all

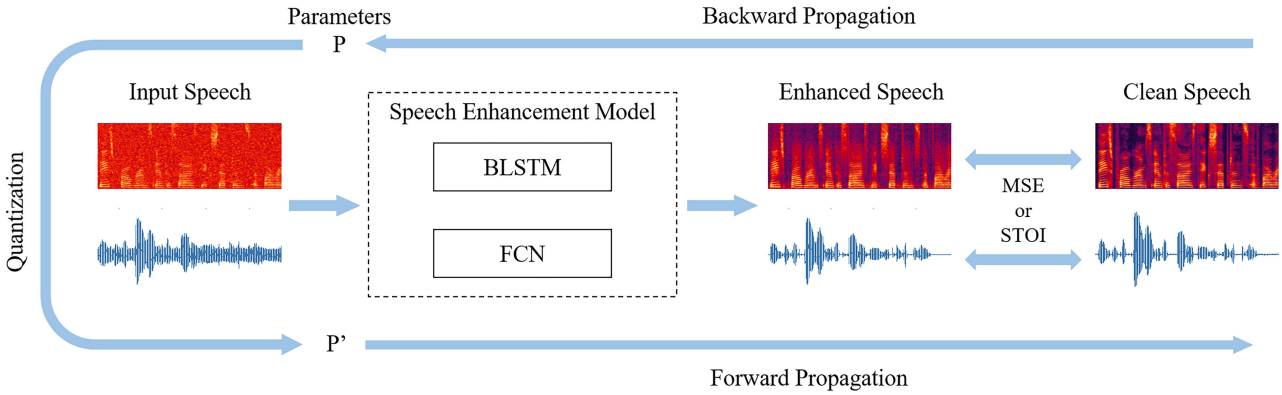

Fig. 3. An overview of the DNN-based speech enhancement systems and the training procedure with the proposed SEOFP-NET technique. For generalization, we tried both magnitude spectrogram and raw-waveform as the input data. We also used BLSTM and FCN to illustrate that our SEOFP-NET can be used in different kinds of the model architectures. For evaluating the loss between the enhanced speech signals and the clean speech signals, we used either MSE or STOI as the objective function after the forward propagation.

parameters of the DNN-based speech enhancement model are forced to use a fixed number of bits in the training phase.

Fig. 3 shows an overview of the DNN-based speech enhancement systems and training procedure with the proposed SEOFP-NET technique. After backward propagation in (k)-th iteration, all single-precision floating-point parameters P are quantized to P' by our proposed SEOFP strategy. The quantized parameters P' are then used as the new model parameters for forward propagation in the succeeding $(k+1)$-th iteration. During training, the DNN-based speech denoising or dereverberation models learn minimum loss based on quantized parameters. In addition, we attempted to use both magnitude spectrogram and raw waveform as input data for the speech enhancement system structure. To illustrate the generalization of different types of model architectures, BLSTM and FCN are used as speech enhancement models. The MSE or STOI was also used as the objective function for evaluating the loss between enhanced and ground-truth clean speech signals.

B. Fraction Quantization Algorithm

In Fig. 1, 71.875% of the single-precision floating-point memory space (i.e., 23 bits in a 32-bit width representation) is observed to be allocated to the fraction part. However, such a high-precision 23-bit long fraction part is unnecessary for the parameters of DNN models. Hence, in the training phase, the DNN-based speech denoising or dereverberation systems are first quantized in the fraction part of all single-precision floating-point parameters. The quantization algorithm is placed between backward propagation and forward propagation of two adjacent iterations, as mentioned in Section III-A. Besides, the algorithm is applied to all parameters (including weights and biases) in the DNN-models.

Algorithm 1 presents the proposed fraction quantization method. For the input, the algorithm is assigned two input attributes: 1) a DNN model Λ with l layers and 2) a positive integer, x, to indicate the remaining number of bits after the fraction quantization. Please note that Λ is the model after the backward propagation in any iteration, k. For the output, a model Λ', which is quantized with all floating-point parameters in bit width x, is used for the forward propagation in the next iteration, $k+1$. Before the fraction quantization algorithm is applied, a

Algorithm 1: Fraction Quantization.

Input: A model Λ with l layers, $\{L_i | i = 1, 2, \ldots, l\}$. A positive integer x for the width of the valid bits in a single-precision floating-point value.
Output: A quantized model Λ' with all floating-point parameters in bit-width x.

$kernel \leftarrow [1_{31}1_{30}\ldots 1_{31-x+1}0_{31-x}0_{31-x-1}\ldots 0_0]$
for each layer L_i in the model Λ **do**
  for each floating-point parameter P in L_i **do**
    Convert P into a 32-bit binary variable $B[31:0]$
    if $32 > x > 9$ **then**
      $B[32-x] = B[32-x]\ ||\ B[31-x]$
    else if $x = 9$ **then**
      $B[30:23] = B[30:23] + B[22]$
    end if
    $B[31:0] = B[31:0]$ & $kernel[31:0]$
    Convert B back to P'
  end for
end for
return Λ'

global binary variable, $kernel$ with a 32-bit width is defined. The head x bits of the kernel are 1 s, and the latter $32-x$ bits are 0 s. For each layer, L_i, of the model, parameter P is fetched; P is first converted from single-precision floating-point data point into a 32-bit binary variable, B. If x is greater than 9 and less than 32, an OR operation is executed with two operands: $B[32-x]$ and $B[31-x]$; the result then updates the value of bit $B[32-x]$. An OR operation is used to avoid overflow from the fraction segment to the exponent segment. Here, $B[30:32-x]$ possibly contains all 1 s and results in the domino effect of carrying 1. By contrast, if x is equal to 9 (i.e., only the sign and exponent parts are left in the single-precision floating-point value), the exponent value $B[30:23]$ is then added to the value of $B[22]$. The use of rounding arithmetic prevents overflow from the exponent segment to the sign segment. A floating-point value with an exponent consisting of all 1 s (11111111) is an infinite value, ∞, that does not appear in DNN-based speech enhancement models. It is impossible that carrying 1 into the exponent part leads to an overflow to the sign bit; hence, the exponent value,

$B[30:23]$, can be directly rounded. The maximum value of x is 32, which means that quantizing the single-precision floating-point parameters is unnecessary. Finally, the binary variable, B, is masked by the binary $kernel$ and then converted back to the floating-point parameter, P'.

In short, after the backward propagation in one iteration, k, a rounding-like arithmetic is applied to quantize the fraction segment of the single-precision floating-point parameters in the DNN-based speech enhancement model Λ. Then, model Λ' with all floating-point parameters in bit width x is employed for the forward propagation in the next iteration, $k+1$. In addition, after applying the fraction quantization strategy to the proposed DNN-based speech enhancement system, the quantized model, whose parameters are only all composed of the sign and exponent parts (i.e., $x=9$), is found capable of achieving the denoising or dereverberation performance of the original single-precision model. That is, quantizing all 23 bits in the fraction part of the single-precision floating-point format is the limitation of the fraction quantization strategy.

C. Replacement of Floating-Point Multiplier With Integer Adder in Online Inference

After the offline training of a DNN-based speech enhancement system, accelerating the online inference may be attempted. Because of the simpler electronic circuit design, more efficient integer adders may be employed to function as floating-point multipliers for executing floating-point multiplication operations. However, a floating-point value and an integer value considerably differ in their binary formats. Accordingly, a suitable strategy to solve this problem must be developed for the enhanced utterance to remain unchanged after forward propagation. More specifically, all floating-point parameters in the trained speech denoising or dereverberation model must be adjusted to guarantee that the binary result from the integer addition has the same value as that from the floating-point multiplication. The following equation illustrates the target of replacement with adjustment on two floating-point operands, A and B:

$$(A')_2 + (B')_2 = (A)_2 \times (B)_2 \tag{5}$$

where $+$ is an integer addition operation, and $\times$ is a floating-point multiplication operation; A' and B' are two integer addition operands adjusted according to A and B, respectively. In addition, because there are three parts (i.e., $sign$, $exponent$, and $fraction$) in the binary format of a floating-point parameter, these three segments are adjusted individually, as follows:

1) Sign: Overflow handling is inherent in integer adder circuits; hence, the mechanism is employed to assume the XOR operation of sign in the floating-point multiplication. As mentioned in Section II-C, the sign value is either 0 or 1, representing a positive or negative floating-point value, respectively. There are only four sign cases in the XOR operation: $\{0,0\}$, $\{0,1\}$, $\{1,0\}$, and $\{0,0\}$; and the XOR results are 0, 1, 1, and 0 respectively. The results of the three cases ($\{0,0\}$, $\{0,1\}$, and $\{1,0\}$) are observed to be the same as those operated by the integer addition. Hence, two sign operands in these cases can be directly added without any label or modification. For the $\{1,1\}$ case, the addition result is 10, and the overflow that occurs is labeled by the integer adder. The integer adder handles this overflow situation by abandoning 1 and allowing 0 to remain. Therefore, in addition to replacing the XOR operation with addition, the overflow label is removed. In this way, the sign resulting from integer addition is identical to the result that is yielded by floating-point multiplications in all four cases.

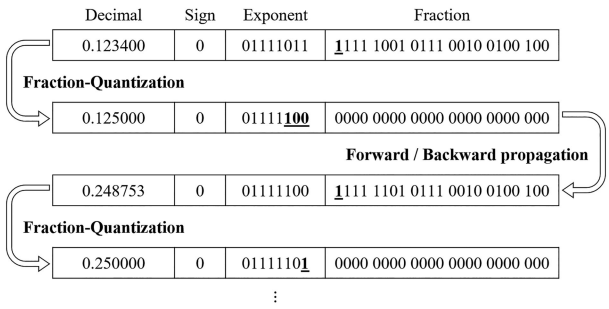

Fig. 4. An example of the off-line training process for a floating-point parameter B. The decimal value of B was 0.123400 in the first iteration. After the rounding-like fraction-quantization, the exponent value of B was carried by 1 and the fraction value became 0. The model then used the updated parameter with value 0.125000 for the next iteration. The algorithm keeps quantizing the model until the end of the training.

2) Fraction: To ensure that the fraction part resulting from the integer addition of A' and B' is the same as that yielded by the floating-point multiplication of A and B, the 23 bits in the fraction part of either A' or B' should all be 0 s. In the online inference, because A is represented as an input value of one layer, it is not adjusted; this means that A' has the same value as A. Therefore, only the fraction value of B is adjusted. The result presented at the end of the previous section indicates that a quantized speech enhancement model may be obtained. The performance of this model is similar to that of the original single-precision model with parameters composed only of the sign and exponent parts after the offline training. An example of the offline training process of the floating-point parameter, B, is shown in Fig. 4. With all B' parameters without the fraction values, the fraction resulting from integer addition is identical to the result obtained by floating-point multiplication.

3) Exponent: There are two problems in adjusting the exponent part: the overflow from the exponent segment to the sign segment and the subtraction using the bias, i.e., 127, for the subtractor, as mentioned in II-D. For the overflow problem, the concept is to avoid the most significant bit (MSB) of the exponent (i.e., the leftmost bit) for both A and B to be 1, allowing the maximum binary value of the exponent segment to become 01111111. Consequently, the maximum addition result of the two operands of the exponent is 10000000, and the sign bit is never affected by the exponent addition. With this constraint, the bit length of the addition result remains at 8. To achieve this goal, all input values and model parameters are normalized in the decimal value range $[-1,1]$. This normalization restricts the binary values of the exponent in the range [00000000,01111111] for the MSB of the exponent to remain 0. Please note that 00000000 and 01111111 are the exponent values of ± 0 and ± 1, respectively. With this method, the overflow from the exponent segment to the sign segment never occurs.

For the second problem, directly increasing the subtraction after the integer-adder replacement increases the number of instructions. More specifically, a floating-point multiplication instruction substituted by integer addition and integer subtraction decelerates the online inference. Accordingly, the subtraction of the bias (127) is divided into two parts: 64 and 63. The reason for the separation is that both 2^{-64} and 2^{-63} are decimal values

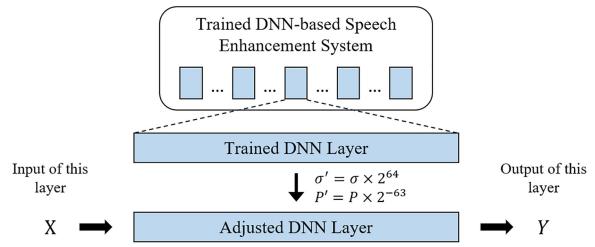

Fig. 5. Adjustment of a DNN layer in a trained DNN-based speech enhancement system. The model's parameters and the standard deviation of normalization are denoted as P and σ respectively. After the off-line training, the σ is multiplied by 2^{64} and the parameters P are divided by 2^{63}. In the on-line inference, the input X is processed by the adjusted DNN layer with new P' and new σ'. The output Y is then passed to the next adjusted DNN layer.

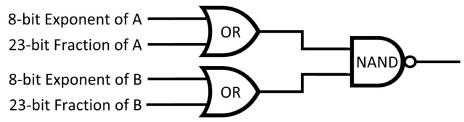

Fig. 6. An efficient computing logic circuit commonly used for determining whether either of the operands is zero in various computing units. The circuit composes of two OR gates followed by an NAND gate. All 31 bits in the exponent and fraction parts of A and B first execute the OR operations. The results of OR gates then execute a NAND operation. Finally, the result of the NAND gate is 1 indicates the multiplication result is zero since either of the operands is zero.

that are extremely smaller than the absolute values of the input and model parameters. The subtractions of 64 and 63 are then distributed to the each of the input values and model parameters.

Fig. 5 illustrates the adjustment of a DNN layer in a trained DNN-based speech enhancement system. The input and output floating-point values of the layer are denoted as X and Y, respectively. In addition, all model parameters are represented by Ps, and σ indicates the standard deviation of normalization. After the offline training, all Ps are divided by 2^{63}, i.e., the exponent values further subtract 63 (00111111); in contrast, σ is multiplied by 2^{64}. Because σ is the denominator, the multiplication of 2^{64} to the denominator is equal to the division of the entire value by 2^{64}. Therefore, the exponent values further subtract 64 (01000000) during the normalization. The input, X, is then processed by the adjusted DNN layer with the new P' and new σ'; and the output, Y, is passed to the next adjusted DNN layer. With this technique, 127 is further subtracted from the exponent values.

A special case exists in the floating-point multiplication, i.e., the zero-operand multiplication. If either of the operands is zero, the result of the floating-point multiplication is zero. For the single-precision floating-point representation, there are two signed zeros, $+0$ and -0, whose 31 bits of the exponent and fraction parts are all 0 s. Fig. 6 shows an efficient computing logic circuit, which is composed of two OR operators followed by an NAND operator; it is commonly used for determining whether either of the operands is zero in various computing units. If one of the OR results is 0 (which means that either A or B is zero), then the result of the NAND gate is 1, indicating that the multiplication result is 0. Otherwise, if both OR results are 1 s, then the result of the NAND gate is 0, indicating that the multiplication result is not 0. Accordingly, this efficient logic is applied to the circuit in the zero-operand multiplication case.

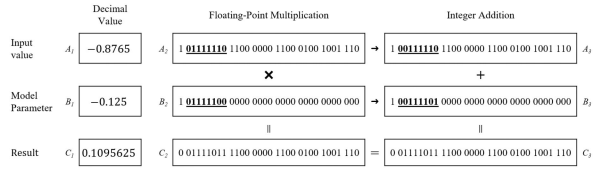

Fig. 7. An example of the conversion of two floating-point multiplication operands for replacing the floating-point multiplier with a integer adder. The decimal value of two floating-points: *Input value* and *model parameter* are -0.8765 (A_1) and -0.125 (B_1); the decimal multiplication result is 0.1095625 (C_1). The binary values of two operands are A_2 and B_2. After the adjustment, the binary values transforms to A_3 and B_3. The multiplication result of A_2 and B_2 by a floating-point multiplier is C_2 which equals to C_3 the addition result of A_3 and B_3 by an integer adder.

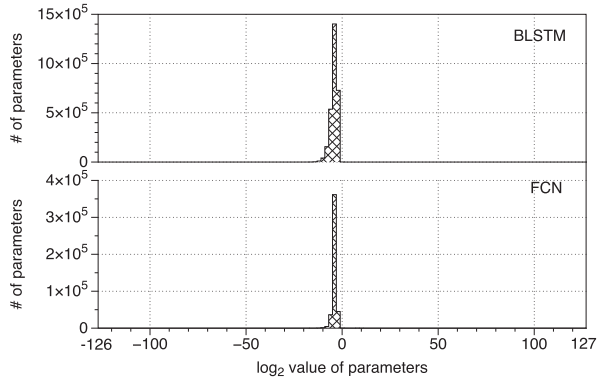

Fig. 8. Value distribution of all parameters in $\log_2$ for BLSTM and FCN. The x-axis is the $\log_2$ values and the y-axis is the number of parameters. The reason for the range $[-126, 127]$ of the x-axis is that -127 and 128 are used for 0 and ∞ respectively in the 8-bit exponent ranging in $[-127, 128]$.

Fig. 7 illustrates an example of the conversion of the two floating-point multiplication operands for replacing the floating-point multiplier with an integer adder.

D. Exponent-Quantization Algorithm

The maximum number of quantized bits for a single-precision floating-point parameter can easily be verified as 23 based on the fraction quantization algorithm presented in Section III-B. After the offline training, 9 bits are left in the sign and exponent parts. Fig. 8 shows the value distribution of all absolute parameters in the BLSTM and FCN models in $\log_2$. Please note that the 8-bit exponent with the bias (i.e., 127) determines an exponent value range in $[-127, 128]$, where -127 and 128 are used for 0 and ∞. Thus, the value range in the x-axis in Fig. 8 is from -126 to 127. All 9 bits in the sign and exponent parts are known to be designed for a wide value range, i.e., from $\pm 2^{-127}$ to $\pm 2^{128}$. However, the normalization process commonly applied to DNN-based models constrains all model parameters within a narrow value range, as shown in Fig. 8. The main reason for applying normalization is to reduce the differences among the parameters. Based on observation, the parameters are further quantized on these 9 bits. The exponent part should further be quantized because of the 1 bit in the sign part. Accordingly, an exponent quantization algorithm based on the value distribution is proposed.

Algorithm 2 illustrates the proposed exponent quantization. For the input, a trained speech enhancement model, Λ, is afforded to the algorithm. For the output, three output attributes

Algorithm 2: Exponent-quantization.

Input: A trained model Λ
Output: The bit-width $width$. An exponent value min in $\log_2$. A quantized model Λ'

Find the MAX and min which are the maximum and minimum decimal exponent values in Λ (except for 0).
$width = Ceil(\log_2((MAX - min + 1) + 1))$
for each parameter P in Λ **do**
  E is the exponent value of P in decimal.
  if $E \neq 0$ **then**
    $E' = E - min + 1$
  end if
  P' with the exponent value E' substitutes for P in Λ'
end for
return $width$, min, and Λ'

are considered: 1) $width$ indicating the number of bits necessary for the exponent to represent all parameters; 2) min denoting the minimum exponent value in the model; and 3) a quantized model, Λ', for exponent quantization. First, the MAX and min, which are the maximum and minimum exponent values in $\log_2$ in Λ (except for zero values) are determined, respectively. Thereafter, the least bit width is calculated through the ceiling function of $\log_2((MAX - min + 1) + 1)$ The reason for determining the latter is that the 00000000 binary value is used to represent the zero value, as explained in the previous paragraph. Next, for each parameter in model λ, the exponent value, E, is fetched from parameter P. If E is not equal to zero, then the new exponent value, E', is calculated by $E - min + 1$, i.e., the new exponent value, E', is the offset between *E* and *min*. The addition of 1 to the end is necessary because min is represented by 1. Finally, with the new exponent value, E', P' is substituted for P in model Λ'. For instance, if the parameter value range is $[\pm 0, \pm 2^{-11}, ..., \pm 2^{2}]$, the MAX and min are 2 and -11 respectively. In this case, only 5 bits (that is $1+\lceil \log_2(2-(-11)+1+1)\rceil$) are required for all parameters. The first 1 bit is for the sign part. The new exponent values, i.e., $E's$ of ± 0, $\pm 2^{-11}$ and $\pm 2^{1}$ are 0, 1, and 13 respectively. Please note that the performance is not affected because the bit length of the exponent part has been reduced without changing the values.

IV. Experiments and Results

This section presents the experimental setup and results of SEOFP-NET on the speech denoising and dereverberation tasks.[2] Section IV-A first describes the experimental setup including the training/testing datasets, model architectures, and performance metrics. Sections IV-B to IV-H describe the conduct of several experiments to compare the SEOFP-NET technique with other strategies. Section IV-B presents the comparison of the proposed rounding-like fraction quantization with a direct removing strategy to show that quantizing the fraction bits without any constraint results in the evident degradation of the speech denoising performance. Sections IV-C and IV-D explain the application of the SEOFP-NET technique to the denoising and dereverberation tasks, respectively, and the performance evaluation of enhanced speech signals. The STOI is also integrated into the objective function to improve the performance of the STOI metric, as discussed in Section IV-E. Section IV-F elaborates on the comparison between the model with the proposed integer adder replacement and the original model in the online inference time. Section IV-G presents the comparison of all the model sizes in the original single-precision floating-point models, models with fraction quantization, and models with fraction-exponent quantization. In addition, a simple cooperation of our quantization and an existing parameter pruning strategy is presented thereafter. Finally, the JND metric, which is applied to evaluate the results of the user study, is presented in Section IV-H.

[2]The codes, pretrained models, and the JND test platform can be accessed via: https://github.com/dwadelin/SEOFP-NET.

A. Experimental Setup

To clearly demonstrate the capability of the proposed SEOFP-NET, extensive experiments were conducted on different model architectures and datasets. The SEOFP-NET is also applied to the denoising and dereverberation tasks, demonstrating that the proposed technique can achieve satisfactory performance on different speech enhancement tasks of regression in speech signal processing. To comprehensively understand the differences in performance among the different speech denoising or dereverberation systems, several metrics are employed to evaluate the quality of the enhanced speech signals. The datasets, model architectures, and evaluation metrics are detailed as follows:

1) Datasets: In the experiments, the TIMIT corpus [52] is used as the dataset for the denoising task, whereas the TMHINT corpus [53] is employed as the dataset for the dereverberation task. To evaluate the results objectively, a mismatch of noises, SNR, and room impulse responses (RIRs) between the training and testing sets is intentionally designed. For the training set of the denoising task, all 4620 utterances from the training set of the TIMIT corpus were used. These utterances were corrupted with 100 different types of noise that are both stationary and non-stationary at eight different signal-to-noise (SNR) levels (from -10 to 25 dB at steps of 5 dB) to generate $4620 \times 100(types) \times 8(SNRs) = 3,696,000$ noisy training utterances. For the testing set of denoising tasks, 100 utterances from the testing set of the TIMIT corpus were used; these were different from the 4620 utterances employed in the training set. These utterances were corrupted by five different noise types (engine, street, two talkers, baby cry, and white) at four different SNR levels (from -6 to 12 dB at steps of 5 dB) to generate $100 \times 5(types) \times 4(SNRs) = 2000$ noisy testing utterances (i.e., 2.2 hours of noisy testing data).

For the dereverberation task, three room conditions were simulated to generate different acoustic characteristics: room 1, room 2, and room 3 with dimensions $4 \times 4 \times 4$ m, $6 \times 6 \times 4$ m, and $10 \times 10 \times 8$ m, respectively. For the dereverberation task training set, 360 utterances of the TMHINT corpus were employed. These utterances were convolved with three different RIRs and three considerations of T_{60}, i.e., 0.3, 0.6, and 0.9 (s) to generate $360 \times 3(T_{60}s) \times 3(RIRs) = 3240$ reverberant training utterances (i.e., 3.2 hours of training data). For the testing set of dereverberation tasks, 120 utterances from the TMHINT corpus are used; these are different from the 360 utterances used in the training set. These utterances were convolved with a single RIR along with three considerations of T_{60}, i.e., 0.4, 0.7, and 1.0 (s) to generate $120 \times 3(T_{60}s) \times 1(RIRs) = 360$ reverberant testing utterances (i.e., 0.4 hours of testing data).

2) Model Architectures: Two different model architectures are used, BLSTM and FCN, as shown in Fig. 3. For the

TABLE II
PESQ SCORES OF ENHANCED SPEECH SIGNALS FROM BLSTM AND FCN USING THE PROPOSED FRACTION-QUANTIZATION ALGORITHM AND DIRECTLY REMOVING WITHIN 6 DIFFERENT BIT-WIDTHS ON DENOISING TASK

	BLSTM		FCN	
Bit-width	Fraction Quantization	Directly Removing	Fraction Quantization	Directly Removing
32	2.1435	2.1435	2.0642	2.0642
26	2.1364	2.1352	2.0743	2.0636
20	2.1252	2.1413	2.0811	2.0743
14	2.1354	2.1364	2.0931	2.0857
10	2.1541	2.1455	2.0544	2.0345
9	2.1124	2.0975	2.0758	1.8595

BLSTM-based speech enhancement systems, the spectrograms of the speech signals were employed as the system input. The speech signals were first parameterized into a sequence of 256-dimensional log-power spectrum features. Then, mapping was performed frame-by-frame using the BLSTM model. This model has two BLSTM layers followed by two fully connected layers. Each BLSTM layer has 257 nodes, and the first fully connected layer has 300 nodes; the second layer is a fully connected output layer. The BLSTM architecture is similar to that employed in [49]. In contrast, for the FCN-based speech enhancement systems, raw-waveform speech signals were directly utilized as the system input/output without further waveform-spectrum conversion. The FCN model has 10 convolutional layers. Each of the first nine layers has 30 size 55 filters; the last layer has only one size 55 filter. The FCN architecture is similar to that used in [66].

3) Evaluation Metrics: To evaluate the performance of speech denoising and dereverberation, two standardized objective evaluation metrics are used: PESQ [54] and STOI [55]. For PESQ, whose score range is from -0.5 to 4.5, a higher value represents better speech signal quality. For STOI, whose score range is from 0 to 1, a higher score represents better speech signal intelligibility. In addition, the JND [56]–[58] is applied to evaluate the response times of participants in determining the similarity between two enhanced speech signals processed by the original single-precision floating-point model and the proposed SEOFP model.

B. Proposed Rounding-Like Strategy Versus Direct Removal Technique for Fraction Quantization

An intuitive method to quantize the fraction bits is to maintain the required number of x bits and directly remove the last $32 - x$ bits in the fraction segment. However, the removal of some bits without considering their effect may result in performance degradation. Accordingly, a rounding-like fraction quantization algorithm is proposed in Section III-B. The performance of this proposed quantization algorithm is compared with that of the direct removal method in the denoising task. Table II summarizes the PESQ scores of the models with six different bit widths (i.e., 32, 26, 20, 14, 10, and 9). Please note that the 32-bit models are the original single-precision floating-point models, and the 9-bit models indicate that all parameters in those models do not have fraction bits. Each PESQ score listed in Table II is the average score in the three noise types and four SNR levels.

The PESQ scores listed in the table are only slightly downgraded when the proposed rounding-like fraction quantization is applied. For example, although the bit width decreased from 32 to 9, the PESQ scores degraded by only 1.45% (from 2.1435 to 2.1124) and -0.56% (from 2.0642 to 2.0758) for BLSTM and FCN, respectively. The negative value, -0.56%, indicates that the performance of the 9-bit quantized FCN model is better than that of the original single-precision floating-point FCN model. However, the PESQ scores are apparently downgraded if several bits when directly removed from the fraction part. For example, although the bit width decreased from 32 to 9, the PESQ scores degraded by only 2.15% (from 2.1435 to 2.0975) and 9.92% (from 2.0642 to 1.8595) for BLSTM and FCN, respectively. The results illustrate the potential of the proposed fraction quantization, which uses a rounding-like strategy to quantize the fraction bits to reduce the approximation error.

C. Denoising Using Fraction Quantization

The results listed in Table II not only show the feasibility of fraction quantization but also suggest that similar denoising performance can still be maintained with only 9 bits (i.e., the sign and exponent bits) left in all model parameters. Table III lists the detailed PESQ and STOI scores for the BLSTM and FCN using the original single-precision floating-point models and the proposed SEOFP-NET models under four specific SNR conditions. Each value is an average score in five noise types (engine, street, two talkers, baby cry, and white). The SEOFP models are quantized by fraction quantization within a 9-bit width. The score reductions are represented as a percentages from the baseline scores to the SEOFP-NET scores. In addition, the PESQ and STOI scores for the unprocessed noisy testing utterances are also listed in the table.

The results in Table III indicate that in applying the SEOFP-NET strategy to the BLSTM-based denoising models, the reduction in the PESQ score is only 1.45% (from 2.1435 to 2.1124), whereas that for the STOI score is only 0.09% (from 0.7529 to 0.7522). Similarly, for the FCN-based denoising models, the reduction in the STOI score is only 2.90% (from 0.7547 to 0.7328); however, the PESQ score improves by 0.56% (from 2.0642 to 2.0758). A possible reason for this improvement is that the single-precision floating-point parameters may be extremely precise in that the trained parameters overfit the training utterances.

Another observation from Table III is that the FCN-based denoising model has suffered more reductions in the STOI scores after the fraction quantization. A possible reason for this phenomenon is that the number of parameters in the FCN is considerably smaller than the number of parameters in the BLSTM; consequently, each parameter performs a more important denoising function. The same slight error resulting from the fraction quantization of a parameter differently affects the BLSTM and FCN denoising models. Nevertheless, the compression rates are approximately $3.56\times$ in both models, indicating that the sizes of DNN-based models could be substantially compressed with slight reductions in the denoising performance. Fig. 9 illustrates the spectrograms and waveforms of a sample utterance in the denoising task. Fig. 9(a) to (d), shows the spectrograms of clean speech, noisy (engine noise), enhanced speech processed by the original FCN, and enhanced speech processed by SEOFP-NET, respectively; and Fig. 9(e) to (g), shows the speech signals in the waveform format.

TABLE III
DETAILED PESQ AND STOI SCORES FOR BLSTM AND FCN USING THE ORIGINAL SINGLE-PRECISION FLOATING-POINT MODELS AND THE PROPOSED SEOFP-NETS UNDER SPECIFIC SNR CONDITIONS. EACH SCORE IS AN AVERAGE SCORE OF THREE NOISE TYPES (ENGINE, STREET, AND TWO TALKERS). THE SCORE REDUCTIONS ARE REPRESENTED IN THE PERCENTAGE FROM BASELINE'S SCORES TO SEOFP-NET'S SCORES

	Noisy		BLSTM				FCN			
			Baseline		SEOFP-NET		Baseline		SEOFP-NET	
SNR(dB)	PESQ	STOI	PESQ	STOI	PESQ	STOI	PESQ	STOI	PESQ	STOI
-6	1.2232	0.5094	1.4986	0.5676	1.4881	0.5685	1.3814	0.5483	1.4443	0.5384
	-	-	+0.2754	+0.0582	+0.2649	+0.0591	+0.1582	+0.0389	+0.2211	+0.0290
	-	-	-	-	-0.70%	+0.16%	-	-	+4.55%	-1.81%
0	1.6218	0.6592	1.9831	0.7280	1.9620	0.7246	1.8427	0.7189	1.8774	0.7001
	-	-	+0.3613	+0.0688	+0.3402	+0.0654	+0.2209	+0.0597	+0.2556	+0.0409
	-	-	-	-	-1.06%	-0.47%	-	-	+1.88%	-2.62%
6	2.0161	0.7996	2.3932	0.8315	2.3612	0.8314	2.3036	0.8403	2.2813	0.8144
	-	-	+0.3771	+0.0319	+0.3451	+0.0318	+0.2875	+0.0407	+0.2652	+0.0148
	-	-	-	-	-1.34%	-0.01%	-	-	-0.97%	-3.08%
12	2.4394	0.9005	2.6991	0.8846	2.6383	0.8842	2.7291	0.9112	2.7003	0.8783
	-	-	+0.2597	-0.0159	+0.1989	-0.0163	+0.2897	+0.0107	+0.2609	-0.0222
	-	-	-	-	-2.25%	-0.05%	-	-	-1.06%	-3.61%
Average	1.8251	0.7172	2.1435	0.7529	2.1124	0.7522	2.0642	0.7547	2.0758	0.7328
	-	-	+0.3184	+0.0357	+0.2873	+0.0350	+0.2391	+0.0375	+0.2507	+0.0156
	-	-	-	-	-1.45%	-0.09%	-	-	+0.56%	-2.90%

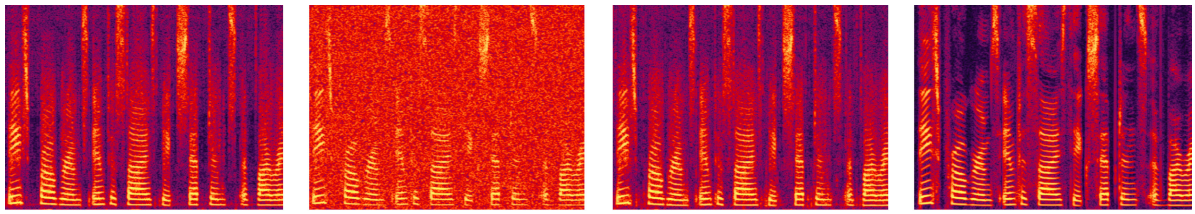

(a) clean spectogram (b) noisy spectogram (c) Baseline spectogram (d) SEOFP-NET spectogram

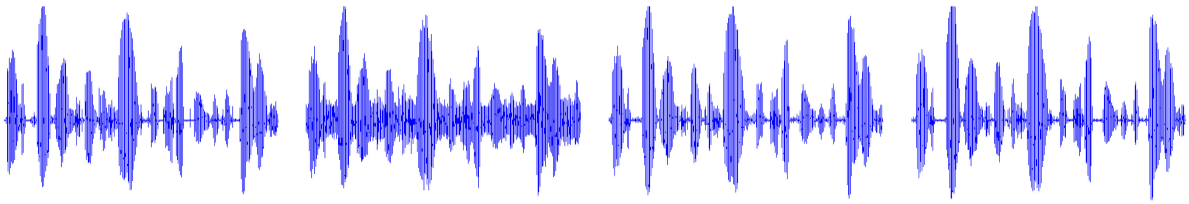

(e) clean raw-waveform (f) noisy raw-waveform (g) Baseline raw-waveform (h) SEOFP-NET raw-waveform

Fig. 9. Spectrograms and waveforms of an example utterance in the denoising task: (a) and (e) clean speech signals; (b) and (f) noisy speech signals (engine noise); (c) and (g) enhanced speech signals by the original single-precision floating-point FCN; (d) and (h) enhanced speech signals by the proposed SEOFP-NET.

D. Dereverberation With Fraction Quantization

To illustrate the capability of speech enhancement tasks of regression in speech signal processing, the proposed SEOFP-NET is applied to a speech dereverberation task. Table IV summarizes the details of the PESQ and STOI scores in the dereverberation by the original single-precision floating-point FCN model and SEOFP-NET under the three specific reverberation conditions of T_{60}. The score reductions are represented as a percentage from the baseline scores to the SEOFP-NET scores. The PESQ and STOI scores in the unprocessed reverberant testing utterances are listed in the table. The results indicate that in applying the SEOFP-NET strategy to the FCN-based dereverberation model, the STOI score was only reduced by 6.07% (from 0.6951 to 0.6529). In contrast, the PESQ score improved by approximately 1.69% (from 1.9661 to 1.9994). These results confirm that the proposed SEOFP-NET may also be applied to different types of speech enhancement tasks of regression in speech signal processing to compress the model sizes of

TABLE IV
DETAILED PESQ AND STOI SCORES FOR DE-REVERBERATION ON THE ORIGINAL SINGLE-PRECISION FLOATING-POINT FCN MODEL AND SEOFP-NET UNDER THREE SPECIFIC REVERBERATION CONDITIONS T_{60}

	Reverberant		Baseline		SEOFP-NET	
T_{60}	PESQ	STOI	PESQ	STOI	PESQ	STOI
0.4	2.1887	0.6168	2.3217	0.7925	2.3153	0.7550
	-	-	+0.133	+0.1757	+0.1266	+0.1382
	-	-	-	-	-0.28%	-4.73%
0.7	1.8279	0.4728	1.9086	0.7019	1.9336	0.6495
	-	-	+0.0807	+0.2291	+0.1057	+0.1767
	-	-	-	-	+1.31%	-7.47%
1	1.6531	0.4010	1.6681	0.5908	1.7494	0.5543
	-	-	+0.015	+0.1898	+0.0963	+0.1533
	-	-	-	-	+4.87%	-6.18%
Ave.	1.8899	0.4969	1.9661	0.6951	1.9994	0.6529
	-	-	+0.0762	+0.1982	+0.1095	+0.1561
	-	-	-	-	+1.69%	-6.07%

TABLE V
DETAILED PESQ AND STOI SCORES FOR DENOISING SYSTEMS USING STOI AS THE OBJECTIVE FUNCTION ON THE ORIGINAL SINGLE-PRECISION FLOATING-POINT FCN MODEL AND THE PROPOSED SEOFP-NET

	Noisy		Baseline-S		SEOFP-NET-S	
SNR(dB)	PESQ	STOI	PESQ	STOI	PESQ	STOI
-6	1.2232	0.5094	1.3891	0.5946	1.3803	0.5853
	-	-	+0.1659	+0.0852	+0.1571	+0.0759
	-	-	-	-	-0.63%	-1.56%
0	1.6218	0.6592	1.8280	0.7537	1.7511	0.7272
	-	-	+0.2062	+0.0945	+0.1293	+0.0680
	-	-	-	-	-4.21%	-3.52%
6	2.0161	0.7996	2.2649	0.8675	2.1132	0.8414
	-	-	+0.2488	+0.0679	+0.0971	+0.0418
	-	-	-	-	-6.70%	-3.01%
12	2.4394	0.9005	2.6937	0.9288	2.4893	0.9122
	-	-	+0.2543	+0.0283	+0.0499	+0.0117
	-	-	-	-	-7.59%	-1.79%
Ave.	1.8251	0.7172	2.0439	0.7862	1.9335	0.7665
	-	-	+0.2188	+0.0690	+0.1084	+0.0494
	-	-	-	-	-5.40%	-2.50%

TABLE VI
AVERAGE INFERENCE TIMES AND SPEED UP RATIOS FOR BLSTM, FCN-10, FCN-12 USING THE BASELINE MODELS AND THE PROPOSED SEOFP-NETS. THE INFERENCE TIME (PER SECOND OF TESTING UTTERANCE) ARE IN UNITS OF MILLISECONDS

Model		Metric	Average	Inference Time (ms)	Speed Up Ratio
BLSTM	Baseline	PESQ	2.1435	78.711	-
		STOI	0.7529		
	SEOFP NET	PESQ	2.1124	66.020	1.192×
		STOI	0.7522		
FCN_{10}	Baseline	PESQ	2.0642	110.691	-
		STOI	0.7547		
	SEOFP NET	PESQ	2.0758	91.308	1.212×
		STOI	0.7328		
FCN_{12}	Baseline	PESQ	2.0583	134.035	-
		STOI	0.7543		
	SEOFP NET	PESQ	2.1074	110.709	1.211×
		STOI	0.7326		

speech dereverberation systems with only marginal degradations in performance. Another observation is that the PESQ scores improved under most reverberation conditions, i.e., T_{60}, whereas the STOI scores were reduced under all reverberation conditions in the considered scenarios. A possible reason is that the objective function used in this dereverberation model is the MSE, which has a higher positive correlation with PESQ than with STOI. The rounding-like approximation, which maintains the MSE loss while quantizing the model in training, results in lower performance degradation in PESQ than in STOI.

E. Integration of STOI Metric Into Objective Function

The results in Table III and IV indicate that the improvement of enhanced speech in the STOI metric compared with that in PESQ is unclear. Moreover, the reductions (yielded by the original single-precision floating point FCN model and proposed SEOFP-NET) in STOI exceed the reductions in PESQ. The main reason is similar to the explanation provided regarding the previous experiment. The MSE objective function used for training the speech denoising and dereverberation models has a high positive correlation with PESQ; however, the loss function is not sufficient for the STOI metric. Thus, in this experiment, the STOI metric is integrated into the objective function of denoising models. A framework similar to that used in [66] was employed.

Table V summarizes the PESQ and STOI scores in the denoising systems using STOI as the objective function in the original single-precision floating-point FCN model and the proposed SEOFP-NET. Compared with the FCN scores listed in Table III, the denoising systems with STOI as the objective function achieved higher improvements in the STOI scores. Consider the improvement under the -6 dB SNR condition as an example (i.e., second row, -6 dB of FCN in Tables III and V). The Baseline-S and SEOFP-NET-S models improved by 0.0852 and 0.0759 in the STOI metric, respectively, whereas the baseline and SEOFP-NET models only improved by 0.0389 and 0.0290, respectively. In addition, the score reductions (from the baseline model to the SEOFP model) in STOI are smaller than the score reductions in PESQ. For example, in quantizing the parameters, the reduction in the PESQ score was 5.40% (from 2.0439 to 1.9335); however, the reduction in the STOI score was only 2.50% (from 0.7862 to 0.7665). These results confirm that the STOI optimization is considerably related to achieving speech intelligibility improvement and suggest that applying SEOFP-NET with STOI as the objective function decreases the score reduction in the STOI metric.

F. Acceleration by Replacing Floating-Point Multipliers With Integer Adders for Floating-Point Multiplications

To evaluate the improvement in the inference time, the procedures of the BLSTM and FCN models are simulated using C language on a personal computer with an Intel(R) Core(TM) i7-6700 3.40-GHz CPU. The $clock$ function in the $time.h$ library was also used to evaluate the inference time for speech denoising. In addition, another 12-layer FCN model was created for comparison. Similar to the previous FCN models, the model has 12 convolutional layers with zero padding for the size to be the same as the input. Each of the first 11 layers consists of 30 size 55 filters, and the last layer has only one size 55 filter.

Table VI summarizes the average online inference times and speedup ratios for BLSTM, FCN_{10}, and FCN_{12} using the baseline models and the proposed SEOFP-NETs. The inference times for noisy testing data with an average of 1.3 hours (i.e., 1200 testing utterances) are given in units of millisecond. The results in the table indicate that the inference times are significantly reduced by SEOFP-NET. The acceleration rates of inference time are 1.192× (from 78.711 to 66.020), 1.212× (from 110.691 to 91.308), and 1.211× (from 134.035 to 110.709) for the BLSTM, FCN_{10}, and FCN_{12}, respectively. That is, the inference time of DNN-based speech denoising systems can simply be accelerated by the proposed SEOFP-NET strategy without expensive and complicated hardware accelerators.

The results in Table VI further indicate that although FCN_{12} SEOFP-NET has two more convolutional layers than the FCN_{10} baseline model, their inference times are virtually the same. More specifically, the average inference time of FCN_{12} SEOFP-NET is approximately 110.691 ms (per second of the testing utterance); this approximates the 110.709-ms average inference time of the FCN_{10} baseline model. However, for the performance metrics, FCN_{12} SEOFP-NET outperforms the FCN_{10} baseline model in PESQ and has a STOI score similar to that of the latter. The result suggests that instead of training the

TABLE VII
NUMBER OF PARAMETERS AND THE MODEL SIZES OF THE BLSTM AND FCN USING THE BASELINE SINGLE-PRECISION MODELS, SEOFP-NETS WITH ONLY FRACTION-QUANTIZATION, AND SEOFP-NETS WITH BOTH FRACTION- AND EXPONENT-QUANTIZATION ALGORITHMS. THE MODEL SIZES ARE IN UNITS OF KILOBYTES (KB). THE COMPRESSION RATIOS ARE ALSO LISTED IN THE TABLE

	BLSTM	Compression Ratio	FCN	Compression Ratio
Number of parameters	2,877,929	-	450,301	-
Size of the baseline models with single-precision floating-point (KB)	11,242	-	1,759	-
Size of the SEOFP-NETs with Fraction-Quantization (KB)	3,162	-71.873%	495	-71.859%
Size of the SEOFP-NETs with Fraction-Exponent-Quantization (KB)	2,108	-81.249%	385	-78.113%
Number of parameters of SEOFP FCN model with parameter pruning	-	-	337,725	-83.570%
Size of SEOFP FCN model with parameter pruning (KB)			289	

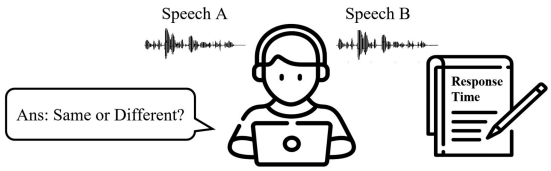

Fig. 10. The environment of the JND user study experiment. For each pair of utterances in the 100-pair A/B Test, the participant listened to two enhanced speech signals and then answer in SAME or DIFF. The response time was recorded to determine the availability of the response.

DNN-based speech denoising system with fewer layers, training the SEOFP-NET with more layers can improve performance without increasing the online inference time.

G. Further Model Compression by Exponent Quantization Algorithm and Existing Parameter Pruning Strategy

Table VII lists the number of parameters and model sizes of the BLSTM and FCN using the original single-precision models, SEOFP-NETs with only the fraction quantization, SEOFP-NETs with both fraction and exponent quantization algorithms, and the combination of SEOFP and parameter pruning. The sizes of all models are in kilobytes (kB). The compression ratios, which represent the size reduction percentages from the baseline models to the SEOFP-NETs, are also listed in the table and calculated by the following equation:

$$Compression\ ratio = \frac{S_{SEOFP} - S_B}{S_B} \times 100\% \qquad (6)$$

where S_{SEOFP} and S_B represent the sizes of baseline models and SEOFP-NETs, respectively.

From the table, the sizes of models with the proposed fraction quantization algorithm compared with those of the baseline models are evidently compressed. The sizes of the SEOFP-NETs with fraction quantization compared with those of the baseline BLSTM and FCN models were reduced to 71.873% (from 11,242 to 3,162) and 71.859% (from 1,759 to 495), respectively. These compression ratios may be attributed to the redundant fraction bits in the single-precision floating-point parameters. To further compress the model sizes, the proposed exponent quantization algorithm was applied to the trained BLSTM-based and FCN-based speech denoising systems, as mentioned in Section III-D. First, the maximum MAX and minimum min exponent values in $\log_2$ of each model were determined. After the exponent quantization, the value set $\{MAX, min, width\}$ of each model were obtained, i.e., $\{0, -23, 5\}$ for the BLSTM-based denoising model, respectively, and $\{10, -26, 6\}$ for the FCN-based denoising model, respectively. The quantized models were also generated by the exponent quantization algorithm. As indicated in the table, the sizes of the SEOFP-NETs with the fraction and exponent quantization algorithms compared with those of the SEOFP-NETs with only the fraction quantization were further compressed.

Compared with the sizes of the baseline models, those of the SEOFP-NETs were reduced by approximately 80.249% (from 11,242 to 2,108) and 78.113% (from 1,759 to 385) for the BLSTM and FCN, respectively. In other words, the model sizes of SEOFP-NETs are only one-fifth of the sizes of the baseline models. Further, the compression ratios may be attributed to the narrow value distribution of all parameter exponents. In addition, to verify that the proposed SEOFP strategy can cooperate with other efficiency strategies to achieve a synergy effect, we combine our quantization strategy with an existing parameter pruning strategy proposed by [80], [81], as shown in Table VII. From the table, the number of parameters in the FCN model reduced from 445,301 to 337,725. The model remaining model size is only 16.43% (from 1,759 to 289 KB). It is also noted that the integration of parameter pruning obtained similar enhancement performances in terms of PESQ and STOI. The result is encouraging for combination of different efficiency methodologies finding the compression limitation of speech enhancement without performance degradation.

H. Just Noticeable Difference

Finally, the JND is employed as the metric for the user study. The JND is the minimum amount of change that can produce a noticeable variation in sensory experience (e.g., sight, hearing, and tactile sense) [56]–[58]. In the human hearing system, the JND is used to measure the difference among similar speech signals (acoustics or sounds). Accordingly, the JND is an appropriate metric for evaluating the difference between the enhanced speech signals yielded by the baseline model and that of the proposed SEOFP-NET. The environment of this JND user study experiment is shown in Fig. 10. In this experiment, six denoising SEOFP-NETs with six different bit widths (i.e., 32, 26, 20, 14, 10, and 9) for the parameters presented in Section IV-B are employed. For the A/B test for 20 participants, 100 pairs of speech signals were prepared; each participant was requested to listen to the same 100 pairs of speech signals. For each pair, one speech was the utterance enhanced by the baseline model, and the other was enhanced by one of the six SEOFP-NETs. Note that if the speech is enhanced by the SEOFP-NET with a

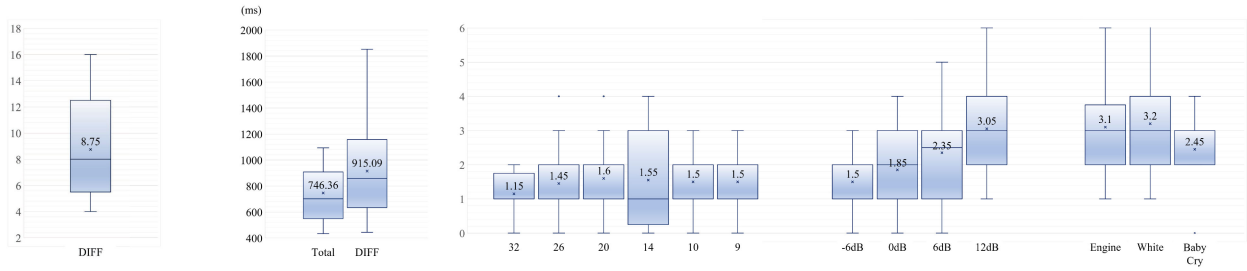

(a) amount of DIFF responses (b) response times (c) amounts of DIFF responses under different conditions

Fig. 11. Statistic box plots of the response times and the amounts of DIFF responses of the 20 participants in the 100-pair enhanced utterances A/B Test. (a) the amount of DIFF responses; (b) the average response times of total 100 pairs and the pairs of DIFF responses are in units of milliseconds; (c) the amount of DIFF responses under the SEOFP-NETs with 6 different bit-widths, 4 different SNR levels, and 3 different noise types.

32-bit width, these two speech signals will be the same because the SEOFP-NET with a 32-bit width is exactly the same as the baseline model. Moreover, both speech signals are under the same SNR condition. After listening to these pairs of speech signals, each participant had to determine whether the speech signals were the same or different by giving the answers $SAME$ or $DIFF$, respectively. The response time for the determining the similarity or difference between the two enhanced speech signals was recorded.

Fig. 11 illustrates the statistical boxplots of the average response times and the amount of time for the 20 participants to reach a DIFF response to the A/B test on the 100 pairs of enhanced utterances; these response times are in milliseconds, as shown in Fig. 11(b). From Fig. 11(a) and 11(b), the average time of the 100 responses is 746.36 ms. This short response time indicates that the JND statistic may be applied. In addition, the average quantity of DIFF responses is only 8.75 out of the 100 pairs of enhanced utterances (as shown in Fig. 11(a)), and the average time of DIFF responses is 915.09 ms. These results have two important implications. First, although reductions in the scores of the standardized objective evaluation metrics (i.e., PESQ and STOI) are observed, as summarized in Tables III, in most pairs of utterances, the two enhanced speech signals sound similar to the listeners. Second, the longer average time of DIFF responses than the average response time of the 100 pairs indicated that the listeners were unable to effortlessly differentiate between the enhanced speech signals from the baseline model and the proposed SEOFP-NETs although they ultimately made the DIFF decision.

To further probe into the scenarios of DIFF responses, the number of DIFF responses under different conditions are categorized into three groups, as shown in Fig. 11(c). The first group consisted of SEOFP-NETs with six different bit widths; the second group had four different SNR levels (-6, 0, 6, and 12); and the last group had three different noise types (engine, white, and baby cry). From the figure, the 8.75 DIFF responses are observed to be evenly distributed among the six different bit widths of the SEOFP-NETs even though the interquartile ranges are slightly different among these models. However, note that the 32-bit model has an average of 1.15 DIFF responses although the A/B enhanced speech signals are actually the same. These erroneous evaluations indicate that the participants were extremely unsure in making the DIFF decisions.

For the different SNR levels, 12 dB is observed to receive the most quantity of DIFF responses, whereas -6 dB had the least quantity among the 100 pairs of enhanced speech signals. A possible reason for this result is that the distortions of the baseline model and SEOFP-NETs are different. The original noisy speech signals with high SNRs inherently have high quality and intelligibility. However, the distortion of enhanced noisy speech signals with high SNRs is more evident than the distortion of enhanced noisy speech signals with low SNRs. Moreover, the various models may cause different distortions while enhancing the noisy speech signals; consequently, the differentiation made by the participants between the two speech signals is based on different distortions. For the different noise types, the average quantity of DIFF responses to the $engine$ noise is 3.1; this approximates 3.2, which is the average quantity of DIFF responses to the $white$ noise. In contrast, the *Baby Cry* noise received the least quantity of DIFF responses among the 100 pairs of enhanced speech signals. These results indicate that a pair of enhanced speech signals with stationary noise can be more facilely differentiated by listeners than a pair with non-stationary noise.

V. Conclusion

In this paper, a novel SEOFP-NET strategy is proposed to compress the model size and accelerate the inference time for speech enhancement tasks of regression in speech signal processing. In the offline training phase, SEOFP-NET compresses model sizes by quantizing the fraction bits of single-precision floating-point parameters. Before the online inference, all parameters are slightly adjusted to accelerate the inference time by replacing the floating-point multiplier logic circuit with an integer-adder logic circuit. The results show that the SEOFP-NET models compared with the baseline models can be significantly compressed by 71.859% to 81.249% and accelerated between 1.192$\times$ and 1.212$\times$ with respect to the inference time. In the meantime, the enhancement performances achieved by SEOFP-NET are similar to that of the baseline models. The results also verify that SEOFP-NET can cooperate with other efficiency strategies to achieve a synergy effect. Moreover, the JND user study indicates that the listeners cannot facilely differentiate between the enhanced speech signals from the baseline models and SEOFP-NETs. The promising results suggest that the DNN-based speech enhancement algorithms with the SEOFP-NET technique can be suitably applied to lightweight embedded devices.

REFERENCES

[1] K. Simonyan and A. Zisserman, "Very deep convolutional networks for large-scale image recognition," in *Proc. Int. Conf. Learn. Representations*, 2015.

[2] K. He, X. Zhang, S. Ren, and J. Sun, "Deep residual learning for image recognition," in *Proc. IEEE Conf. Comput. Vis. Pattern Recognit.*, 2016, pp. 770–778.

[3] P. Luo, Y. Tian, X. Wang, and X. Tang, "Switchable deep network for pedestrian detection," in *Proc. IEEE Conf. Comput. Vis. Pattern Recognit.*, 2014, pp. 899–906.

[4] X. Zeng, W. Ouyang, and X. Wang, "Multi-stage contextual deep learning for pedestrian detection," in *Proc. Int. Conf. Comput. Vis. Workshop*, 2013, pp. 121–128.

[5] P. Sermanet, K. Kavukcuoglu, S. Chintala, and Y. LeCun, "Pedestrian detection with unsupervised multi-stage feature learning," in *Proc. IEEE Conf. Comput. Vis. Pattern Recognit.*, 2013, pp. 3626–3633.

[6] A. Graves, A. Mohamed, and G. Hinton, "Speech recognition with deep recurrent neural networks," in *Proc. IEEE Int. Conf. Acoust., Speech Signal Process.*, 2013, pp. 6645–6649.

[7] G. Hinton *et al.*, "Deep neural networks for acoustic modeling in speech recognition: The shared views of four research groups," *IEEE Signal Process. Mag.*, vol. 29, no. 6, pp. 82–97, Nov. 2012.

[8] L. Deng *et al.*, "Recent advances in deep learning for speech research at microsoft," in *Proc. IEEE Int. Conf. Acoust., Speech Signal Process.*, 2013, pp. 8604–8608.

[9] J. Li, L. Deng, R. Haeb-Umbach, and Y. Gong, *Robust Automatic Speech Recognition: A Bridge to Practical Applications*. Elsevier, Orlando, FL, USA: Academic, 2015.

[10] Z.-Q. Wang and D. Wang, "A joint training framework for robust automatic speech recognition," *IEEE/ACM Trans. Audio, Speech, Lang. Process.*, vol. 24, no. 4, pp. 796–806, Apr. 2016.

[11] C. Donahue, B. Li, and R. Prabhavalkar, "Exploring speech enhancement with generative adversarial networks for robust speech recognition," in *Proc. IEEE Int. Conf. Acoust., Speech Signal Process.*, 2018, pp. 5024–5028.

[12] T. Ochiai, S. Watanabe, T. Hori, and J. R. Hershey, "Multichannel end-to-end speech recognition," in *Proc. 34th Int. Conf. Mach. Learn.*, 2017, pp. 2632–2641.

[13] D. Michelsanti and Z.-H. Tan, "Conditional generative adversarial networks for speech enhancement and noise-robust speaker verification," in *Proc. Interspeech*, 2017, pp. 2008–2012.

[14] S. Shon, H. Tang, and J. Glass, "VoiceID loss: Speech enhancement for speaker verification," in *Proc. Interspeech*, 2019, pp. 2888–2892.

[15] Y. Lan, Z. Hu, Y. C. Soh, and G.-B. Huang, "An extreme learning machine approach for speaker recognition," *Neural Comput. Appl.*, vol. 22, no. 3/4, pp. 417–425, 2013.

[16] P. C. Loizou, *Speech Enhancement: Theory and Practice*, *2nd ed*. Boca Raton, FL, USA: CRC Press, Inc., 2013.

[17] S. Boll, "Suppression of acoustic noise in speech using spectral subtraction," *IEEE Trans. Acoust., Speech, Signal Process.*, vol. 27, no. 2, pp. 113–120, Apr. 1979.

[18] P. Scalart and J. V. Filho, "Speech enhancement based on a priori signal to noise estimation," *Proc. IEEE Int. Conf. Acoust., Speech, Signal Process. Conf. Proc.*, vol. 2, pp. 629–632, 1996.

[19] Y. Ephraim and D. Malah, "Speech enhancement using a minimum-mean square error short-time spectral amplitude estimator," *IEEE Trans. Acoust., Speech, Signal Process.*, vol. 32, no. 6, pp. 1109–1121, Dec. 1984.

[20] Y. Hu and P. C. Loizou, "A subspace approach for enhancing speech corrupted by colored noise," in *Proc. IEEE Int. Conf. Acoust., Speech, Signal Process.*, 2002, pp. I-573–I-576,.

[21] A. Rezayee and S. Gazor, "An adaptive klt approach for speech enhancement," *IEEE Speech Audio Process.*, vol. 9, no. 2, pp. 87–95, Feb. 2001.

[22] P. Huang, S. D. Chen, P. Smaragdis, and M. Hasegawa-Johnson, "Singing-voice separation from monaural recordings using robust principal component analysis," in *Proc. IEEE Int. Conf. Acoust., Speech Signal Process.*, 2012, pp. 57–60.

[23] N. Zheng and X.-L. Zhang, "Phase-aware speech enhancement based on deep neural networks," *IEEE/ACM Trans. Audio, Speech, Lang. Process.*, vol. 27, no. 1, pp. 63–76, Jan. 2019.

[24] D. Liu, P. Smaragdis, and M. Kim, "Experiments on deep learning for speech denoising," in *Proc. Interspeech*, 2014, pp. 2685–2689.

[25] J. Qi, H. Hu, Y. Wang, C.-H. H. Yang, S. M. Siniscalchi, and C.-H. Lee, "Exploring deep hybrid tensor-to-vector network architectures for regression based speech enhancement," in *Proc. Interspeech*, 2020, pp. 76–80.

[26] J. Qi, H. Hu, Y. Wang, C.-H. H. Yang, S. M. Siniscalchi, and C.-H. Lee, "Tensor-to-vector regression for multi-channel speech enhancement based on tensor-train network," in *Proc. IEEE Int. Conf. Acoust., Speech Signal Process.*, 2020, pp. 7504–7508.

[27] D. Wang and J. Chen, "Supervised speech separation based on deep learning: An overview," *IEEE/ACM Trans. Audio, Speech, Lang. Process.*, vol. 26, no. 10, pp. 1702–1726, Oct. 2018.

[28] K.-S. Oh and K. Jung, "Gpu implementation of neural networks,"*Pattern Recognit.*, vol. 37, no. 6, pp. 1311–1314, 2004.

[29] D. Strigl, K. Kofler, and S. Podlipnig, "Performance and scalability of gpu-based convolutional neural networks," in *Proc. 18th Euromicro Conf. Parallel, Distrib. Netw.-Based Process.*, 2010, pp. 317–324.

[30] H. Jang, A. Park, and K. Jung, "Neural network implementation using cuda and openmp," in *Proc. Digit. Image Comput., Techn. Appl.*, 2008, pp. 155–161.

[31] M. Courbariaux, Y. Bengio, and J.-P. David, "Binaryconnect: Training deep neural networks with binary weights during propagations," in *Proc. Int. Conf. Neural Inf. Process. Syst.*, 2015, pp. 3105–3113.

[32] Y. Gong, L. Liu, M. Yang, and L. Bourdev, "Compressing deep convolutional networks using vector quantization," in *Proc. Int. Conf. Learn. Representations*, 2015.

[33] A. Zhou, A. Yao, Y. Guo, L. Xu, and Y. Chen, "Incremental network quantization: Towards lossless CNNs with low-precision weights," in *Proc. Int. Conf. Learn. Representations*, 2017.

[34] P. H. Hung, C. H. Lee, S. W. Yang, V. S. Somayazulu, Y. K. Chen, and S. Y. Chien, "Bridge deep learning to the physical world: An efficient method to quantize network," in *Proc. IEEE Workshop Signal Process. Syst.*, 2015, pp. 1–6.

[35] K. Tan and D. Wang, "Towards model compression for deep learning based speech enhancement," *IEEE/ACM Trans. Audio, Speech, Lang. Process.*, vol. 29, pp. 1785–1794, May 2021, doi: 10.1109/TASLP.2021.3082282.

[36] X. Sun, Z.-F. Gao, Z.-Y. Lu, J. Li, and Y. Yan, "A model compression method with matrix product operators for speech enhancement," *IEEE/ACM Trans. Audio, Speech, Lang. Process.*, vol. 28, pp. 2837–2847, Oct. 2020, doi: 10.1109/TASLP.2020.3030495

[37] Y. Lecun, L. Bottou, Y. Bengio, and P. Haffner, "Gradient-based learning applied to document recognition," *Proc. IEEE Proc. IRE*, vol. 86, no. 11, pp. 2278–2324, 1998.

[38] A. Krizhevsky *et al.*,*Learning Multiple Layers of Features from Tiny Images*. Citeseer, 2009.

[39] Y. Netzer, T. Wang, A. Coates, A. Bissacco, B. Wu, and A. Ng, "Reading digits in natural images with unsupervised feature learning," *NIPS Workshop Deep Learn. Unsupervised Feature Learn.*, 2011.

[40] A. Krizhevsky, I. Sutskever, and G. E. Hinton, "Imagenet classification with deep convolutional neural networks," *Proc. 25th Int. Conf. Neural Inf. Process. Syst.*, vol. 1, pp. 1097–1105, 2012.

[41] C. Szegedy *et al.*, "Going deeper with convolutions," in *Proc. IEEE Conf. Comput. Vis. Pattern Recognit.*, 2015, pp. 1–9.

[42] K. Hwang and W. Sung, "Fixed-point feedforward deep neural network design using weights 1, 0, and −1," in *Proc. IEEE Workshop Signal Process. Syst.*, 2014, pp. 1–6.

[43] F. Seide, H. Fu, J. Droppo, G. Li, and D. Yu, "1-bit stochastic gradient descent and its application to data-parallel distributed training of speech dnns," in *Proc. Interspeech*, 2014, pp. 1058–1062.

[44] R. Prabhavalkar, O. Alsharif, A. Bruguier, and L. McGraw, "On the compression of recurrent neural networks with an application to LVCSR acoustic modeling for embedded speech recognition," in *Proc. IEEE Int. Conf. Acoust., Speech Signal Process.*, 2016, pp. 5970–5974.

[45] S. Han *et al.*, "Ese: Efficient speech recognition engine with sparse LSTM on FPGA," in *Proc. ACM/SIGDA Int. Symp. Field-Programmable Gate Arrays*, 2017, pp. 75–84.

[46] Y. Lin, S. Han, H. Mao, Y. Wang, and W. Dally, "Deep gradient compression: Reducing the communication bandwidth for distributed training," in *Proc. Int. Conf. Learn. Representations*, 2018.

[47] Y. Wang, J. Li, and Y. Gong, "Small-footprint high-performance deep neural network-based speech recognition using split-VQ," in *Proc. IEEE Int. Conf. Acoust., Speech Signal Process.*, 2015, pp. 4984–4988.

[48] J. H. Ko, J. Fromm, M. Philipose, I. Tashev, and S. Zarar, "Precision scaling of neural networks for efficient audio processing," 2017, *arXiv:1712.01340*.

[49] H. Sun and S. Li, "An optimization method for speech enhancement based on deep neural network," in *Proc. IOP Conf. Ser., Earth Environ. Sci.*, IOP Publishing, 2017, Art. no. 012139.
[50] H. Erdogan, J. R. Hershey, S. Watanabe, and J. L. Roux, "Phase-sensitive and recognition-boosted speech separation using deep recurrent neural networks," in *Proc. IEEE Int. Conf. Acoust., Speech Signal Process.*, 2015, pp. 708–712.
[51] Z. Chen, S. Watanabe, H. Erdogan, and J. R. Hershey, "Speech enhancement and recognition using multi-task learning of long short-term memory recurrent neural networks," in *Proc. Interspeech*, 2015, pp. 1–5.
[52] J. Long, E. Shelhamer, and T. Darrell, "Fully convolutional networks for semantic segmentation," in *Proc. IEEE Conf. Comput. Vis. Pattern Recognit.*, 2015, pp. 3431–3440.
[53] J. S. Garofolo, L. Lamel, W. M. Fisher, J. G. Fiscus, and D. S. Pallett, "DARPA TIMIT acoustic-phonetic continous speech corpus CD-ROM. NIST speech disc 1-1.1," NASA STI/Recon, Tech. Rep. N, vol. 93, 1993, Art. no. 27403.
[54] M. Huang, "Development of Taiwan mandarin hearing in noise test" Department of speech language pathology and audiology, National Taipei University of Nursing and Health science, 2005.
[55] I.-T. Recommendation, "Perceptual evaluation of speech quality (PESQ): An objective method for end-to-end speech quality assessment of narrow-band telephone networks and speech codecs," Rec. ITU-T P. 862, Jan. 2001.
[56] C. H. Taal, R. C. Hendriks, R. Heusdens, and J. Jensen, "An algorithm for intelligibility prediction of time-frequency weighted noisy speech," *IEEE Trans. Audio, Speech, Lang. Process.*, vol. 19, no. 7, pp. 2125–2136, Sep. 2011.
[57] D. McShefferty, W. M. Whitmer, and M. A. Akeroyd, "The just-noticeable difference in speech-to-noise ratio," *Trends Hear.*, vol. 19, 2015, Art. no. 2331216515572316.
[58] D. Mcshefferty, W. Whitmer, and M. Akeroyd, "The just-meaningful difference in speech-to-noise ratio," *Trends Hear.*, vol. 20, 2016, Art. no. 2331216515626570.
[59] P. Manocha, A. Finkelstein, R. Zhang, N. J. Bryan, G. J. Mysore, and Z. Jin, "A differentiable perceptual audio metric learned from just noticeable differences," in *Proc. Interspeech*, 2020, pp. 2852–2856.
[60] X. Lu, Y. Tsao, S. Matsuda, and C. Hori, "Speech enhancement based on deep denoising autoencoder," in *Proc. Interspeech*, 2013, pp. 436–440.
[61] Y. Xu, J. Du, L. R. Dai, and C. H. Lee, "A regression approach to speech enhancement based on deep neural networks," *IEEE/ACM Trans. Audio, Speech, Lang. Process.*, vol. 23, no. 1, pp. 7–19, Jan. 2015.
[62] S.-W. Fu, Y. Tsao, and X. Lu, "SNR-aware convolutional neural network modeling for speech enhancement," in *Proc. Interspeech*, 2016, pp. 3768–3772.
[63] B. Xia and C. Bao, "Wiener filtering based speech enhancement with weighted denoising auto-encoder and noise classification," *Speech Commun.*, vol. 60, pp. 13–29, 2014.
[64] M. Kolbk, Z.-H. Tan, J. Jensen, M. Kolbk, Z.-H. Tan, and J. Jensen, "Speech intelligibility potential of general and specialized deep neural network based speech enhancement systems," *IEEE/ACM Trans. Audio, Speech, Lang. Process.*, vol. 25, no. 1, pp. 153–167, Jan. 2017.
[65] S.-W. Fu, T.-Y. Hu, Y. Tsao, and X. Lu, "Complex spectrogram enhancement by convolutional neural network with multi-metrics learning," in *Proc. IEEE 27th Int. Workshop Mach. Learn. Signal Process.*, 2017, pp. 1–6.
[66] S.-W. Fu, Y. Tsao, X. Lu, and H. Kawai, "Raw waveform-based speech enhancement by fully convolutional networks," in *Proc. Asia-Pacific Signal Inf. Process. Assoc. Annu. Summit Conf.*, 2017, pp. 006–012.
[67] S.-W. Fu, T.-W. Wang, Y. Tsao, X. Lu, and H. Kawai, "End-to-end waveform utterance enhancement for direct evaluation metrics optimization by fully convolutional neural networks," *IEEE/ACM Trans. Audio, Speech, Lang. Process.*, vol. 26, no. 9, pp. 1570–1584, Sep. 2018.
[68] S. Pascual, A. Bonafonte, and J. Serra, "Segan: Speech enhancement generative adversarial network," in *Proc. Interspeech*, 2017, pp. 3642–3646.
[69] A. van den Oord *et al.*, "Wavenet: A generative model for raw audio," in *Proc. 9th ISCA Workshop on Speech Synthesis Workshop*, 2016, p. 125.
[70] K. Wang, B. He, and W.-P. Zhu, "Caunet: Context-aware u-net for speech enhancement in time domain," in *Proc. IEEE Int. Symp. Circuits Syst.*, 2021, pp. 1–5.
[71] J. Lin, S. Niu, A. J. van Wijngaarden, J. L. McClendon, M. C. Smith, and K.-C. Wang, "Improved speech enhancement using a time-domain GAN with mask learning," in *Proc. Interspeech*, 2020, pp. 3286–3290.
[72] F. Xiao, J. Guan, Q. Kong, and W. Wang, "Time-domain speech enhancement with generative adversarial learning," 2021, *arXiv:2103.16149*.
[73] A. Pandey and D. Wang, "Dense CNN with self-attention for time-domain speech enhancement," *IEEE/ACM Trans. Audio, Speech Lang. Proc.*, pp. 1270–1279, Jan. 2021.
[74] M. Miyoshi and Y. Kaneda, "Inverse filtering of room acoustics," *IEEE Trans. Acoust., Speech, Signal Process.*, vol. 36, no. 2, pp. 145–152, Feb. 1988.
[75] J. L. Flanagan, J. D. Johnston, R. Zahn, and G. W. Elko, "Computer-steered microphone arrays for sound transduction in large rooms," *J. Acoustical Soc. Amer.*, vol. 78, no. 5, pp. 1508–1518, 1985.
[76] J. Flanagan, A. Surendran, and E. Jan, "Spatially selective sound capture for speech and audio processing," *Speech Commun.*, vol. 13, no. 1, pp. 207–222, 1993.
[77] X. Feng, Y. Zhang, and J. Glass, "Speech feature denoising and dereverberation via deep autoencoders for noisy reverberant speech recognition," in *Proc. IEEE Int. Conf. Acoust., Speech Signal Process.*, 2014, pp. 1759–1763.
[78] T. Ishii, H. Komiyama, T. Shinozaki, Y. Horiuchi, and S. Kuroiwa, "Reverberant speech recognition based on denoising autoencoder," in *Proc. Interspeech*, 2013, pp. 3512–3516.
[79] *IEEE Standard for Binary Floating-Point Arithmetic*, I. of Electrical and E. Engineers, ANSI/IEEE Std 754–1985, 1985.
[80] M. Abadi *et al.*, "TensorFlow: Large-scale machine learning on heterogeneous systems," 2015.
[81] C.-T. Liu, Y.-H. Wu, Y.-S. Lin, and S.-Y. Chien, "Computation-performance optimization of convolutional neural networks with redundant kernel removal," in *Proc. IEEE Int. Symp. Circuits Syst.*, 2018, pp. 1–5.
[82] J.-Y. Wu, C. Yu, S.-W. Fu, C.-T. Liu, S.-Y. Chien, and Y. Tsao, "Increasing compactness of deep learning based speech enhancement models with parameter pruning and quantization techniques," *IEEE Signal Process. Lett.*, vol. 26, no. 12, pp. 1887–1891, Dec. 2019.

Yu-Chen Lin received the B.S. and Ph.D. degrees in computer science and information engineering from National Taiwan University, Taipei, Taiwan, in 2015 and 2021, respectively. He is currently a Senior Engineer with Computing and Artificial Intelligence Technology Group, MediaTek Inc., Hsinchu, Taiwan. His research interests include efficient deep learning algorithms, deep learning compiler, operating systems, embedded systems, and speech signal processing.

Cheng Yu received the B.S. degree from the Department of Electronics Engineering, National Chiao Tung University, Hsinchu, Taiwan, in 2016, and the M.S. degree from the Graduate Institute of Electronics Engineering, National Taiwan University, Taipei, Taiwan, in 2019. He is currently a Research Assistant with the Research Center for Information Technology Innovation, Academia Sinica, Taipei, Taiwan. His research interests include speech signal processing, bio-signal processing, multimedia signal processing, computational compactness, and deep learning.

Yi-Te Hsu received the B.S. degree in electrical engineering from National Taiwan University, Taipei, Taiwan, in 2016, and the M.S. degree in computer science from Johns Hopkins University, Baltimore, MD, USA in 2020. He is currently a Machine Learning Engineer with Otter.ai, working on developing speech and language technology.

Szu-Wei Fu received the M.S. and Ph.D. degrees from the Graduate Institute of Communication Engineering and the Department of Computer Science and Information Engineering, National Taiwan University, Taipei, Taiwan, in 2014 and 2020, respectively. He is currently an Applied Scientist with Microsoft, Vancouver, BC, USA. His research interests include speech processing, speech enhancement, machine learning, and deep learning.

Yu Tsao (Senior Member, IEEE) received the B.S. and M.S. degrees in electrical engineering from National Taiwan University, Taipei, Taiwan, in 1999 and 2001, respectively, and the Ph.D. degree in electrical and computer engineering from the Georgia Institute of Technology, Atlanta, GA, USA, in 2008. From 2009 to 2011, he was a Researcher with the National Institute of Information and Communications Technology, Tokyo, Japan, where he engaged in research and product development in automatic speech recognition for multilingual speech-to-speech translation. He is currently a Research Fellow (Professor) and the Deputy Director with the Research Center for Information Technology Innovation, Academia Sinica, Taipei, Taiwan. His research interests include assistive oral communication technologies, audio coding, and bio-signal processing. He is currently an Associate Editor for the IEEE/ACM TRANSACTIONS ON AUDIO, SPEECH, AND LANGUAGE PROCESSING and IEEE SIGNAL PROCESSING LETTERS.

Tei-Wei Kuo (Fellow, IEEE) received the B.S.E. degree in computer science from National Taiwan University, Taipei, Taiwan, in 1986 and the Ph.D. degree from the University of Texas at Austin, Austin, TX, USA in 1994. He is currently a Lee Shau Kee Chair Professor of information engineering, Advisor to President (Information Technology), and the Dean of College of Engineering, City University of Hong Kong, Hong Kong. Since August 2009, he has also been a Distinguished Professor with the Department of Computer Science and Information Engineering, National Taiwan University, where he was an Interim President during 2017–2019 and an Executive Vice President for Academics and Research during 2016–2019. He has more than 300 technical papers published in international journals and conferences. His research interests include embedded systems, non-volatile-memory software designs, neuromorphic computing, and real-time systems. He is a Fellow of the ACM and U.S. National Academy of Inventors. He is an Executive Committee Member of IEEE TC on Real-Time Systems (TCRTS). He was the recipient of the numerous awards and recognition, including the Humboldt Research Award in 2021, Outstanding Technical Achievement and Leadership Award from IEEE TC on Real-Time Systems and the Distinguished Leadership Award from IEEE TC on Cyber-Physical Systems both in 2017. He is the founding Editor-in-Chief of the *ACM Transactions on Cyber-Physical Systems* (2015–2021) and an Associate Editor for the *IEEE Design & Test Magazine* and a program committee member of many top conferences. He was the recipient of many best paper awards, including ACM/IEEE CODES+ISSS 2019 and ACM HotStorage 2021.